FIRST-PRINCIPLES STUDY OF CO_2 REDUCTION ON MO_2C

by

Xi Peng

B.S. Chemical Engineering, University of Mississippi, 2015

Submitted to the Graduate Faculty of

Swanson of Engineering in partial fulfillment

of the requirements for the degree of

Master of Science

University of Pittsburgh

2017

UNIVERSITY OF PITTSBURGH

SWANSON SCHOOL OF ENGINEERING

This thesis was presented

by

Xi Peng

It was defended on

June 14, 2017

and approved by

J Karl Johnson, Ph.D., W. K. Whiteford Professor
Department of Chemical and Petroleum Engineering

Goetz Veser, Ph.D., Nickolas A. DeCecco Professor
Department of Chemical and Petroleum Engineering

Thesis Advisor: Giannis Mpourmpakis, Assistant Professor
Department of Chemical and Petroleum Engineering

FIRST-PRINCIPLES STUDY OF CO_2 REDUCTION ON MO_2C

Xi Peng, M.S.

University of Pittsburgh, 2017

Periodic Density Functional Theory (DFT) calculations are widely used to study the interactions between reagents and catalysts, as well as to understand the reaction mechanisms occurring on the catalyst surface. In this work, we investigated the CO_2 adsorption, activation and reduction to CO on (1) pristine, (2) K-promoted, and (3) oxygen-covered (001) orthorhombic Molybdenum carbide (β-Mo_2C) surfaces. We calculated the CO_2 interaction with both surface terminations of β-Mo_2C, Mo-terminated and C-terminated, and we found a thermodynamically feasible chemisorption and dissociation of CO_2 on the Mo-terminated surface. The activation energy for CO_2 dissociation on β-Mo_2C (001) surface was found to be 16.8 kcal/mol. The presence of surface promoter atom, potassium (K), enhanced the binding of CO_2, and lowered the activation barrier for CO_2 dissociation from 16.8 kcal/mol to 14.0 kcal/mol. Due to the high oxophilicity of the (001) Mo_2C surface, we further investigated the CO_2 adsorption and dissociation profile on O-covered (001) Mo_2C (simulating experimental conditions), and we found that CO_2 can still adsorb and dissociate on β-Mo_2C (001) surface, even in the presence of surface oxygen up to 0.5ML. As O-coverage increases, the activation barrier for CO_2 dissociation increases. Our results rationalize a series of experimental observations.

TABLE OF CONTENTS

LIST OF TABLES

LIST OF FIGURES

PREFACE

First, I want to say thank you to my thesis advisor, Dr. Giannis Mpourmpakis, for all the patience and guidance he gives me. Without his support and mentoring, I would not be able to overcome the obstacles. I would also like to thank Dr. Mudit Dixit, who gives me tons of guidance and training with my calculations, and helps me understanding theory into a deeper level. Also, I want to say great thank you to all the students in our research group: Ms. Natalie Austin, Mr. Pavlo Kostetskyy, Mr. Michael Taylor, Mr. James Dean. Their selfless support helps me go through my days in graduate school, and their great enthusiasm in science will always be a motivation to me to keep up pace with them.

Last, but not least, I would like to express my love to my friends and family; without your support and encouragement, I would never become who I am today.

1.0 INTRODUCTION

The atmospheric concentration of carbon dioxide (CO_2) increasing steadily since the past century. CO_2 is one of the major contributors to the greenhouse effect, therefore, several environmental concerns are associated with its excess presence in the atmosphere.[1-4] Countries around the globe have been announcing and amending regulations to control CO_2 emission.[5] In 2013, environmental organizations around the world reported that a critical level of CO_2 concentration of 400 ppm had been reached.[6] The fact that the amount of CO_2 being produced is greater than CO_2 being removed impairs the effectiveness of the measurements taken by human society. As increasing amount of CO_2 is inevitable as our society develops, more problems associated with CO_2 are yet to come. Therefore, solutions that are effective and efficient in removing CO_2 from the atmosphere are in urgent need more than ever.[7] In spite of several problems associated with CO_2, due to its low cost, abundance, nontoxicity, and nonflammable nature, it is still a very attractive renewable C_1 feedstock for manufacturing several valuable chemicals, fuels, and materials.[8-11] Researchers have made several attempts to achieve the goal of removing CO_2 from the atmosphere: in general, these methodologies can be grouped into two categories—CO_2 capture, and CO_2 transformation.[7]

1.1 CO_2 CAPTURE

CO_2 capture, is based on the idea that CO_2 can be selectively captured and "trapped" in systems in a safe, stable, and efficient manner. [12] The concept of CO_2 capture is closely related to other concepts such as CO_2 storage, and CO_2 capture can be achieved by either absorption (gas molecules permeate/diffuse into absorbents), or adsorption (adhesion of gas molecule onto the surface of adsorbents), as described in Figure 1. [13] Some of the vastly applied/investigated methods for CO_2 capture by both absorption and adsorption are introduced in the following section.

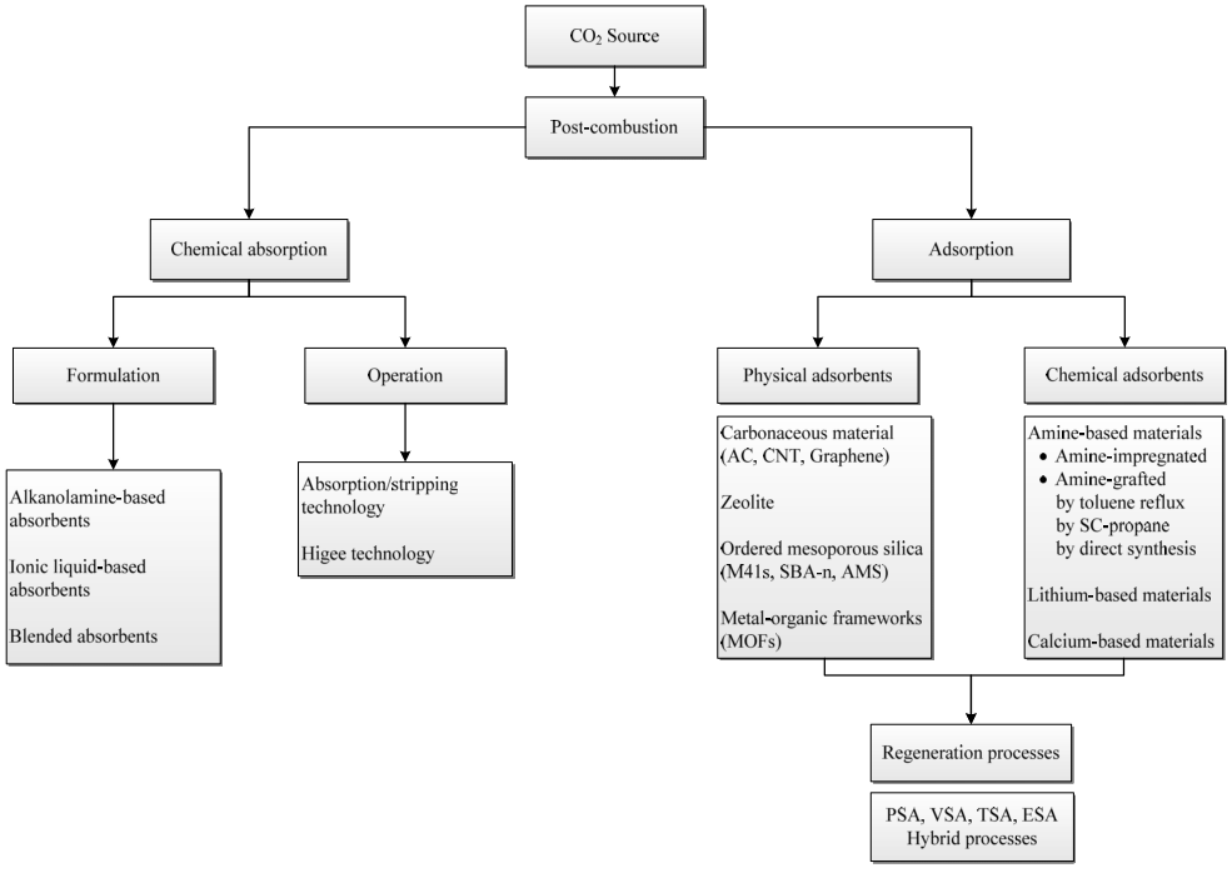

Figure 1: Flow diagram for CO_2 capture by absorption and adsorption. (Figure was obtained from ref: [13])

1.1.1 CO_2 capture by absorption

Traditionally, chemical absorption is carried out by using liquid amine-based absorbent, which can undergo chemical reactions and therefore stabilize CO_2 and eventually reach the goal of "CO_2 capture".[14] A typical chemical absorption process contains an absorber and a stripping column, and by flowing a gas mixture containing CO_2 and liquid absorbent co-currently or counter-currently, CO_2 removal from the gas mixture is achieved. Followed by the CO_2 adsorption, the CO_2-rich absorbent enters the stripping column for thermal regeneration. Subsequently, pure CO_2 releases from the column, and undergoes compression for storage and transportation.[13] The absorption/stripping process is considered as one of the most matured technologies for CO_2 capture, and has been commercialized for many decades[13], yet exhibiting several disadvantages. One significant limitation of CO_2 capture by this process is that no more than 10 wt% of CO_2 can be absorbed in such systems[15]. Other limitations include high equipment corrosion rate, high amine degradation rate,[16] and high energy consumption[17]. These drawbacks associated with absorption process drive researchers and engineers to search for alternative approaches to achieve the goal of CO_2 capture.[16]

Among the others, Ionic liquids (IL) are promising absorbents that have been extensively used in catalysis and synthesis because of their unique properties including low vapor pressure, high thermal stability, and non-toxicity.[18] ILs containing amino-functional groups are particularly important due the large CO_2 absorbing capabilities.[19] The fact that ILs can be synthesized with the desired properties gives researchers much flexibility in developing ILs for wide range of industrial applications including CO_2 capture.[20] However, their high viscosity (slow diffusion) leads to very slow absorption (low rate of absorption) of CO_2 which leads to slow kinetics of the adsorption process.[21] Dealing with this major drawback of ILs used in CO_2

capture, researchers proposed that by mixing of ILs with organic compounds (i.e., alkanolamine), the viscosity of mixture can be controlled without compromising the capability of capturing CO_2. However, this approach still has all the other problems associated with organic compounds including the volatility issues.[22]

High Gravity (HiGee) technology is an innovative method which employs the high centrifugal field using a rotating packed bed (RPB). This method involves to the enhancement in momentum, heat, and mass transfer.[23] RPB has been used in various unit operation processes including desorption[24], dehydrogenation[13], and synthesis of nanoparticles[25], and has been proposed as capable of capturing CO_2.[26, 27] By using aqueous solutions (such as NaOH) in the RPB, it was found that the CO_2 adsorption rate was significantly enhanced compared to the adsorption rates of traditional packed bed columns.[13] However, some of the limitations of the most matured adsorption/stripping process, such as high maintenance and operating costs, also exist here, and thus limit the application of HiGee technology in large industrial scale.

1.1.2 CO_2 capture by adsorption

Due to the fact that traditional absorption processes using the liquids have several disadvantages including low CO_2 loading, low CO_2 absorption rate, and high energy consumption, researchers have been searching for alternatives to achieve the goal of CO_2 capture. Adsorption by solid materials, has been regarded as a promising alternative because of their higher stability under wide temperature ranges and decrease in waste production.[28] Materials such as carbon based, and zeolite based adsorbents have high surface area and large pore volume for interaction with CO_2 gas molecules, but the adsorbents-adsorbates interaction is usually very weak (physisorption), and CO_2 molecules are easily detached from the adsorbates

under optimal conditions.[29] Zeolites are considered to be good candidates for CO_2 adsorption. These are porous crystalline materials, usually containing periodic array of TO_4 tetrahedra (T = Si or Al). Several research reports show a great and increasing promise of these materials. [30] The molecular-sized cavities and large pores inherently existing in zeolitic structures enable the zeolites to selectively adsorb molecules (such as CO_2 molecules) by size and polarity.[31] However, experimental studies revealed a substantial decrease in CO_2 uptake at elevated temperatures (higher than 373 K) or under humid conditions,[31,32] and thus zeolites are considered to be efficient in CO_2 capture only under mild conditions.[30] Another type of materials, alkali metal carbonated based adsorbents, are capable of capturing CO_2 by undergoing reversible chemical reactions with CO_2, but their durability under industrial operating conditions are yet to be discovered.[28] Other materials such as Metal Organic Frameworks (MOFs), Zeolitic Imidazole Frameworks (ZIFs) (a subclass of MOFs) have been under spotlights in recent years as good candidate for separation and storage of CO_2. These represent a class of materials which have high thermal stability[33], adjustable chemical functionality[34], and highly ordered structures.[35] The high surface area presented in MOFs, which can reach up to an extraordinary value of 3000 m^2g^{-1}, [36,37] exceeded the previously reported materials with high surface areas, such as zeolites (904 m^2g^{-1}).[38] The highly-complicated frameworks in the structures of MOFs give them intrinsic capabilities of selectively adsorbing and storing small gas molecules, and their adjustable chemical functionality gives MOFs endless potential in applications.[30] ZIFs have been experimentally tested in applications such as separation of similar size molecules such as CO_2 and CO, and have been reported to be able to selectively capture CO_2 from the mixture with a much higher selectivity compared to other state-of-the-art materials such as BPL carbon [39].

1.2 CO_2 TRANSFORMATION

Instead of storage of CO_2 through the approaches that were discussed in the last section, another approach is to transform CO_2 into useful chemicals, such as long chain hydrocarbons by hydrogenation.[40] The molecular CO_2 molecule is linear in its ground state. Due to the inherent polarity of C-O bonds in CO_2, the carbon atom acts as an electrophile whereas the oxygen atoms act as nucleophiles. However, CO_2 is a very stable molecule with a strong C=O bond strength of 192 kcal/mol, and therefore any reaction relating to CO_2 conversion will have to overcome the C=O bond cleavage[41]. The conversion of CO_2 is often limited by its strong bond strength. However, high energy materials such as hydrogen or organometallics are often capable to convert CO_2 to useful chemicals.[10] One of the promising routes for CO_2 utilization is to convert CO_2 to carbon monoxide(CO), which can be used to obtain valuable hydrocarbons via Fischer-Tropsch process.[11]

In industry, CO_2 reforming of methane[42] (described in Equation (1-1)), one approach to convert CO_2 to CO, has been used to adjust the feed for Fischer-Tropsch process (FT), a process that utilizes CO and H_2 gas mixture to produce liquid hydrocarbons. [43]

$$CO_2 + CH_4 \rightarrow 2\ CO + 2\ H_2 \qquad (1\text{-}1)$$

The overall process for CO_2 reforming of methane is an endothermic reaction (ΔHr = +59.1 kcal/mol), and many studies had investigated different metal catalysts including Rh, Ru, Pd, Ir, for this process. It was reported that Rh and Ru exhibit the highest conversion of CO_2, but these catalysts are too expensive to be applied in industrial scale productions.[36] Direct polymerization of CO_2 (Equation (1-2)) is another approach to convert CO_2 into higher hydrocarbons, and even

though the overall reaction is exothermic, the fully dissociation of CO_2 requires large energy input, and thus have been considered not to be practical in industry. However, CO_2 can be converted into CO via reverse water-gas-shift reaction (RWGS) (Equation (1-3)) , and CO can then be hydrogenated using the FT process to produce long chain hydrocarbons (Equation (1-4)).[44] The most commonly used catalysts in industry for FT processes are slight variations of Fe and Co-based catalysts, these catalysts however, have several limitations. One of the major problems include the poisoning of the Fe-based catalysts by the produced water during the FT process,[43] and therefore the reactivity of the catalysts are impaired after a certain period. Co-based catalysts are comparatively water tolerant and show a relatively high activity for the RWGS reaction.[45] The products from FT process when co-feeding CO_2 almost always has a high methane (CH_4) selectivity instead of higher hydrocarbon selectivity.[46] Other traditional metal catalysts such as Pt, Ru, Pd exist, but due to their high cost, they have rarely been used in industrial scale productions.[45] CO_2 is a promising renewable C_1 feed for manufacturing numerous high-value chemicals fuels and materials,[8,9] due to its high abundance, searching for new catalysts that can convert CO_2 in a more efficient manner is in urgent need.

$$CO_2 + 3\ H_2 \rightarrow (CH_2) + 2\ H_2O \qquad \Delta Hr = -30.6\ kcal/mol \qquad (1\text{-}2)$$

$$CO_2 + H_2 \rightarrow CO + H_2O \qquad \Delta Hr = +\ 9.1\ kcal/mol \qquad (1\text{-}3)$$

$$n CO + (2n+1)H_2 \rightarrow C_nH_{2n+2} + nH_2O \qquad \Delta Hr = -39.7\ kcal/mol \qquad (1\text{-}4)$$

In the previous studies relating to Fe-based FT catalysts, researchers had identified that iron carbides are important active phases in Fe-based catalysts during FT synthesis.[47] Other studies also showed that on Co-based catalysts, the chain growth in FT synthesis occurs at the carbide

site.[44] In recent years, plenty of studies have shown that metal carbides have high catalytic activity: Experimental and theoretical studies have shown that transition metal carbides (TMCs) can act as catalysts as well as supports for metal nanoparticles in various reactions, and in many cases they show even better activity than traditional metal catalysts.[48,49,50,51,52] Considering the high activity and relatively lower cost of TMCs compared to traditional metal catalysts, the interaction of CO_2 with TMC surfaces is of marked interest. [53, 54] The work done by Rodriguez *et al*. has shown that CO_2 can be activated on hexagonal α-Mo_2C (001) and orthorhombic β-Mo_2C (001) (C-terminated) surfaces, and undergoes C-O bond dissociation on β-Mo_2C (001) (Mo-terminated) surface. [49] Porosoff *et al*. have demonstrated that Mo_2C is an active catalyst for CO_2 conversion, and the active phase of Mo_2C was found to be the carbide phase.[11]

Pistonesi *et al*. investigated the effects of surface additives on the binding of molecules on the Mo_2C surfaces. By investigating K-doped Mo_2C surfaces, they showed that the addition of potassium (K) atoms promotes CO adsorption.[55] These findings suggest that TMCs can find application in CO_2 hydrogenation, however, a fundamental understanding of catalytic properties of TMCs is still lacking, especially towards elucidating the detailed reaction mechanisms, and catalysts structure under reaction conditions activation and dissociation.

In this thesis, the adsorption behavior of CO_2 on β-Mo_2C (001) as well as the effects of K promoter in the reaction mechanism was investigated using Density Functional Theory (DFT) calculations.

1.3 THEORETICAL BACKGROUND

In DFT, according to the Hohenbergy-Kohn (H-K) theorem, the ground state properties of a many-electron system can be uniquely determined by an electron density that depends on three spatial coordinates. However, the H-K theorems has limitations due to the fact that a universal functional form of the density functional that provides this minimum energy is not known exactly, especially the energies of interacting electrons. Most DFT calculations are carried out using the Kohn-Sham (KS) DFT, where the challenges of presenting energies of interacting electrons within the density is treated as a static external potential that is mapped onto a non-interacting system of electrons moving in a common effective potential using fictitious orbitals. The overall ground-state density of the system is identical to the real system and then simply becomes the sum of densities of the occupied orbitals

$$\rho(r) = \sum |\psi n\,(r)|^{2} \tag{1-5}$$

The energy functional in KS-DFT is

$$E[\rho] = Ts\,[\rho] + \int V\text{ext}\,(r)\rho(r)dr + J[\rho] + Exc[\rho] \tag{1-6}$$

where Ts represents the kinetic energy of the non-interacting elections, which is the sum of the kinetic energies of individual electrons. The integral represents the electrostatic interaction of the electron density with an external potential V_{ext}. J represents the Hartree repulsion energy, and E_{xc} is the exchange-correlation energy for all electron-electron interactions.

In general, solving Schrodinger's equation is the approach of the wavefunction-based *ab initio* methods to study the atomistic interactions of the many-body problems of electronic structures at the fundamental level. The approach is very complicated because the wavefunction of the many-particle system depends on the position, i.e., coordinates of all the individual particles, and thus, for the systems containing large number of electrons, solving Schrodinger's

equation becomes not feasible. DFT provides a compromise between the system size and computational cost, and can be applied to systems containing many electrons. The most important point for the actual applications of KS-DFT is the functional E_{xc}, which is not known exactly, and approximations are needed. Local-Density Approximation (LDA), which assumes that the exchange correlation energy at each point in the system is the same as that of a uniform electron gas of the same density, provides approximation to the exchange-correlation energy. Yet LDA is considered to be a crude approximation, although it gives reliable results for many cases. LDA played an important role in the construction of the more sophisticated approximation: generalized gradient approximation (GGA), which counteracts the overestimation of binding of LDA. Instead of LDA which assumes that the density can be treated as a uniform electron gas, GGA considers the gradient of electron density, which is more accurate in approximation because density undergoes rapid changes in molecules. In many applications, GGA provides a substantially improved description of the ground state properties, in particular for 3d transition metals. In the present thesis, the Vienna Ab Initio Simulation Package (VASP) is used, which is a powerful and popular *ab initio* program. VASP has been employed to a wide range of problems and materials including bulk systems, surfaces, and interfaces.

2.0 METHODOLOGY

Density Functional Theory (DFT) calculations were performed using the Vienna Ab Initio Simulation Package (VASP).[56] The Perdew-Burke-Ernzerhof (PBE) exchange-correlation functional was employed with generalized gradient approximation (GGA). [57] The crystal structure of β-Mo_2C has an orthorhombic ground state structure with the space group (Pbcn) and lattice parameters of a = 6.022 Å, b = 5.195 Å, and c = 4.725 Å. [58] By applying geometry optimizations based on minimization of the total energy of the unit cell, the DFT lattice parameters are obtained: a = 6.071 Å, b = 5.250 Å, and c = 4.749 Å, which are in good agreement with experimental obtained lattice parameters. The (001) facet of β-Mo_2C is the closest-packed surface, and due to the symmetry of the β-Mo_2C bulk unit cell, the (001) facet can be either Mo-terminated, or C-terminated surface. For all the studies relating to β-Mo_2C (001) surface, a (2×2) supercell was employed. For both terminated surfaces, the supercells of the slab model have 32 atoms of molybdenum (Mo), and 16 atoms of carbon (C), with a cell dimension of 12.15 Å×10.50 Å×14.55 Å. The vacuum space was set to 10 Å in all calculations. For K-promoted β-Mo_2C(001), one K atom was placed on the top layer at different sites, and after geometry optimization, the site that exhibited the strongest binding to K atom was selected for further calculations (K-promoted β-Mo_2C(001) surface). To study the effect(s) of oxygen coverage, several possible oxygen binding sites were considered to find the most energetically preferential sites for oxygen atoms to bind to the surface. Including the clean surface (0ML

coverage), 5 different oxygen coverage was investigated: 0.25ML, 0.50ML, 0.75ML, 1.00ML, and 1.25ML, and CO_2 adsorption behavior on these systems were studied. The kinetic energy cutoff was set to 415 eV, [49] and the convergence criteria to 10E-6 eV for the total electronic energy and 0.01 eV $Å^{-1}$ for the forces acting on atoms and the k-point mesh was 5x5x1 k-point grid generated by Monkhorst-Pack scheme.[59] The Climbing Image-Nudged Elastic Band (CI-NEB) method[60] has been applied to locate transition states in the CO_2 dissociation pathway. During geometry optimization, the bottom two layers were fixed in their bulk positions and all the other atoms were fully relaxed. Vibrational frequencies on the adsorbates were performed to verify local minima and transition states (presence of one imaginary mode).

Two different CO_2 adsorption configurations on the surfaces were considered: horizontal and perpendicular to the surface. In addition, different sites (top and hollow) were taken into consideration for CO_2 adsorption. The binding energy (BE) is calculated as:

$$BE_{(adsorbate)} = E_{(surface + adsorbate)} - E_{(surface)} - E_{(adsorbate)} \quad (2\text{-}1)$$

Where $E_{(surface + adsorbate)}$ is the total electronic energy of the surface with the adsorbed CO_2, $E_{(surface)}$ is the corresponding energy of the clean surface (without any adsorbate), and $E_{(adsorbate)}$ is that of the CO_2 molecule.

In this work, we applied DFT calculations to investigate the CO_2 adsorption and dissociation on β-Mo_2C, and to understand the effect of K-doping on CO_2 adsorption and dissociation on the same systems. Under experimental conditions, the metal carbide surface exposed can turn into oxy-carbide, and therefore CO_2 adsorption on varying O-coverage surfaces was investigated as well. The findings in this work are in excellent agreement with the findings provided by the experimental collaborators at Naval Research Laboratory (NRL).

3.0 CO_2 ADSORPTION ON MOLYBDENUM CARBIDE

Our experimental collaborator from NRL conducted a series of experiments and demonstrated that potassium-promoted Mo_2C is a low-cost, stable, and highly-selective catalyst for RWGS. Their EDS mapping of the catalyst were showed that in $Mo_2C/\gamma\text{-}Al_2O_3$, Mo atoms are evenlly distributed, while on $K\text{-}Mo_2C/\gamma\text{-}Al_2O_3$, a large segragation between Mo and Al was noted, and K is preferrentially found in Mo-rich domains. These findings suggested that K might affect the electronic properties of the on Mo_2C phase. In conversion of CO_2 on catalysts, their experiments showed that with the addition of 2 wt% K to $Mo_2C/\gamma\text{-}Al_2O_3$, the selectivity towards CO was improved significantly, and also showed that a significant improvement in catalytic stability with the addition of K. Futhermore, they showed that as K doping increases, selectivity of CO increases. With lower or no K doping, CH_4 is produced in significant amounts. The apparent activation barrier for CO formation under RWGS conditions at 5 different temperatures between 270 and 330 °C was also studied for both $Mo_2C/\gamma\text{-}Al_2O_3$ and $K\text{-}Mo_2C/\gamma\text{-}Al_2O_3$, and from their calculations, the activation barriers for CO formation are 14.0 and 11.4 kcal mol^{-1} for $Mo_2C/\gamma\text{-}Al_2O_3$ and $K\text{-}Mo_2C/\gamma\text{-}Al_2O_3$, respectively. [61]

3.1 CO_2 ADSORPTION ON PRISTINE MO_2C (001) SURFACE

To understand the adsorption of CO_2 on the Mo_2C surface, two different adsorption orientations were considered: the horizontal configuration, with the CO_2 molecule being parallel to the surface, and the perpendicular configuration, where one oxygen atom interacts with the surface atoms. Table 1 summarizes the binding energies (kcal/mol) of the CO_2 molecule on both the Mo- and C- terminated β-Mo_2C (001) surfaces. From our results, the horizontally oriented CO_2 molecule exhibits higher binding energy with the surface compared to that with the perpendicularly orientation. On both C-terminated and Mo-terminated surfaces, the CO_2 adsorption on hollow sites and top C/Mo sites (based on surface termination) were investigated, and the hollow site was found to have stronger binding with CO_2 molecule on both the surfaces. Moreover, CO_2 chemisorption and activation are thermodynamically feasible on the Mo-terminated β-Mo_2C (001) surface, whereas, the CO_2 does not chemisorb on the C-terminated surface as shown in Table 1.

Table 1. Adsorption energy (kcal/mol) of CO_2 on both Mo- and C-terminated β-Mo_2C(001) surface.

Surface	*BE(CO_2 ,phys) kcal/mol*	*BE(CO_2, chem) kcal/mol*
Mo_2C-C terminated	-1.91 (perpendicular) hollow site -2.37 (horizontal) hollow site -0.33 (horizontal) top Mo site	NA
Mo_2C-Mo terminated	-0.27 (perpendicular) hollow site -0.52 (horizontal) hollow site -0.33 (horizontal) top Mo site	-31.40 hollow site -24.31 top Mo site -74.81 (CO* + O*)

The activation of CO_2 on Mo-terminated surface was identified by the bending of the CO_2 molecule, and bond elongation of the C=O bond. Showing in Figure 2: at hollow site (the site that exhibits stronger binding of CO_2), the activated CO_2 had a O-C-O bond angle of 114.5 degrees, and the C-O bond was elongated from 1.16 A (C=O bond length in a gas-phase CO_2 molecule) to 1.34 A.

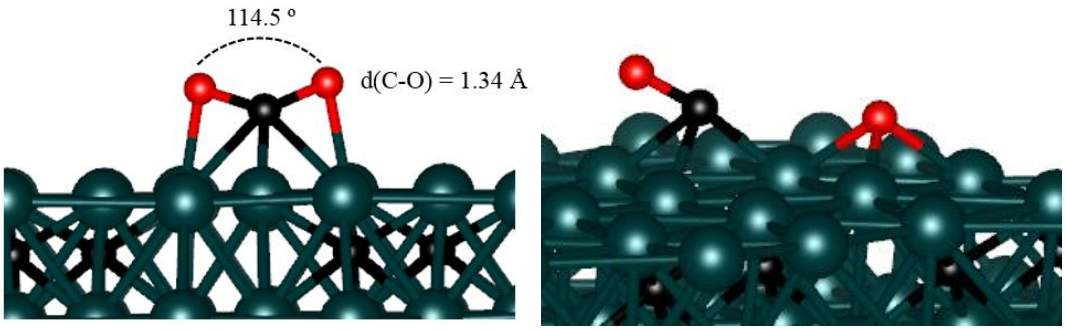

Figure 2: activated CO_2 (left), and dissociated CO_2 (right) on Mo-terminated Mo_2C (001) surface. Color code: cyan-Mo, black-C, red-O.

Since activation of CO_2 is thermodynamically feasible on the Mo-terminated β-Mo_2C (001) surface, we considered whether CO_2 can undergo further dissociation, which involves C=O bond cleavage. Several dissociated CO_2 configurations (CO* and O*) on the Mo-terminated β-Mo_2C (001) surface were studied, and after minimizing the total energy of the systems, the most stable structure which has one oxygen atom bonded to hollow position was obtained as shown in Figure 2. In this dissociated configuration, CO* was attached to the surface with C atom at a hollow position interacting with three surface Mo atoms with an average bond length of 2.1 Å, and C-O length in CO* is 1.28 Å. The BE (CO*+O*) = -74.8 kcal/mol (reference: total energy of the clean surface and CO_2 gas molecule at infinite separation). While the whole process of CO_2 dissociation on the Mo-terminated surface appeared to be thermodynamically feasible, we applied a climbing image-NEB (CI-NEB) calculations to study the kinetics of the reaction, to study the dissociation pathway, and to obtain transition state (T.S.) and associated activation energy. From our result, first, CO_2 barrierlessly activates (-31.4 kcal/mol), and then dissociates to CO* and O*, with an activation barrier of 16.8 kcal/mol. The C-O bond length for the T.S. was 1.92 Å (figure 3). In Figure 4, the dissociation profile of CO_2 on Mo-terminated surface is presented. All of these steps are exothermic with respect to the initial, CO_2 physisorption state.

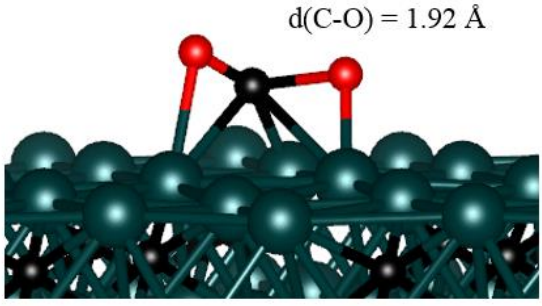

Figure 3: Transition state (T.S.) for CO_2 dissociation on Mo-terminated Mo_2C (001) surface. Color code: grey-C, cyan-Mo, red-O

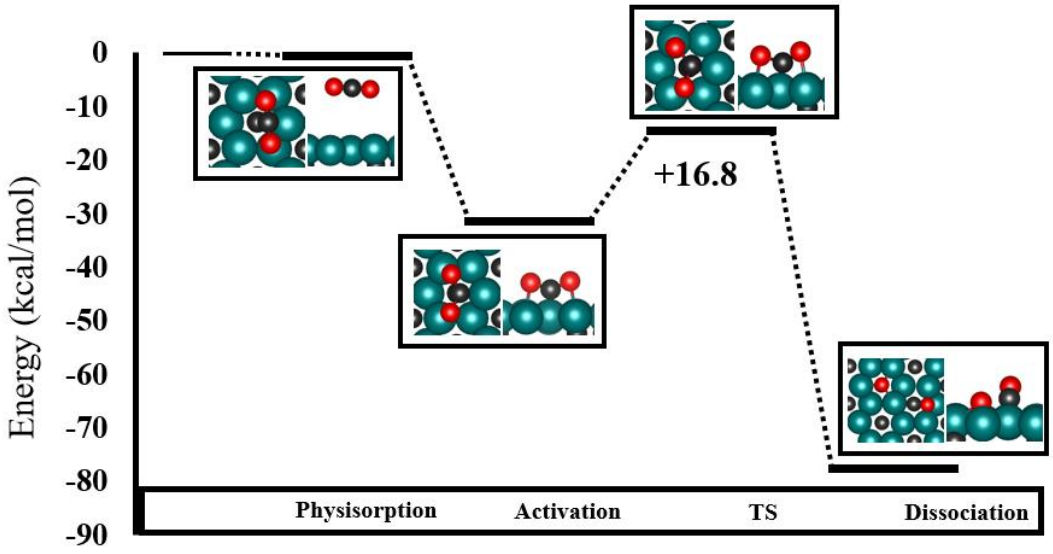

Figure 4: CO_2 dissociation profile on Mo-terminated, β-Mo_2C (001) surface (energy in kcal/mol). Color code: grey-C, cyan-Mo, red-O

3.2 CO_2 ADSOPRTION ON K-PROMOTED MO_2C (001) SURFACE

DFT calculations were performed on K-modified β-Mo_2C(001) surfaces because we also wanted to know how surface adatoms effect adsorption capability of the surface. Similar to that on the pristine surface, CO_2 does not chemisorb on the K-promoted C-terminated surface, but can be activated and dissociated on the K-promoted Mo-terminated surface. Table 2 summarized the calculated CO_2 binding energy on the K-promoted surfaces. The activated CO_2 on the K-doped surface was identified by tracking the change in the CO_2 bond angle and C-O bond length. At the hollow site, the activated CO_2 has a bond angle of 123.5 degrees, and the bond length was

1.35 Å (Figure 5). By directly comparing the BE of CO_2 on pristine and K-promoted surfaces, it becomes clear that the presence of K significantly enhances the CO_2 physisorption on Mo_2C (001) (from -0.5 to -6.5 kcal mol^{-1} at hollow site, from -0.3 to -2.2 kcal/mol at top Mo site), and moderately increases the BE of the chemisorbed states (from -74.8 to -80.9 kcal mol^{-1} for dissociated CO_2, and from -31.4 to -46.6 kcal mol^{-1} for activated CO_2, respectively). The activated CO_2 and dissociated CO_2 are presented in Figure 5.

Table 2:Adsorption energy (kcal/mol) of CO_2 on both K doped Mo- and K doped C-terminated β-Mo2C(001) surface.

Surface	*BE(CO_2 ,phys) kcal/mol*	*BE(CO_2, chem) kcal/mol*
K-Mo_2C-C terminated	-6.17 (horizontal) hollow site -0.85 (horizontal) top Mo site	NA
K-Mo_2C-Mo terminated	-6.97 (horizontal) hollow site -2.19 (horizontal) top Mo site	-46.57 hollow site -42.17 top Mo site -80.90 (CO*+O*)

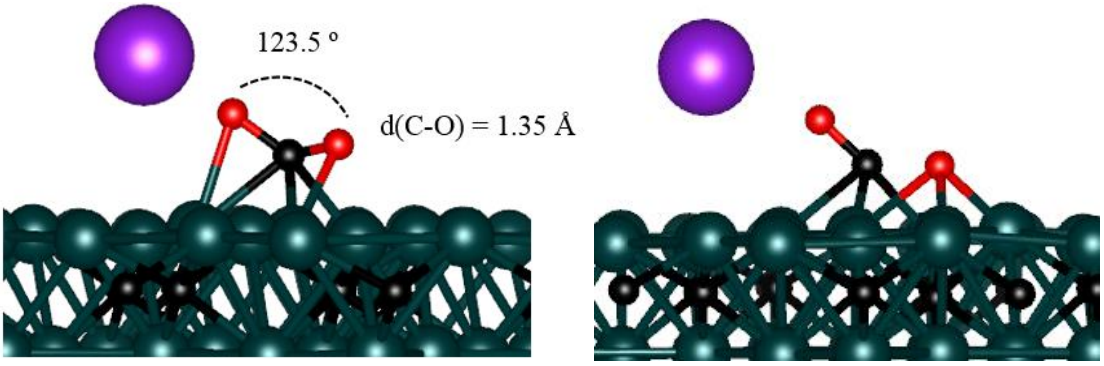

Figure 5: Activated CO_2 (left), and dissociated CO_2 (right) on K doped, Mo-terminated Mo_2C (001) surface. Color code: cyan-Mo, black-C, red-O, purple-K

These energy changes in the presence of K are due to electronic effects. As the DFT calculations suggest (Bader charge analysis), K loses almost one electron, which is delocalized on the surface of the Mo_2C. As a result, the presence of a point charge (K-cation) increases the dipole-dipole interaction character in the CO_2 physisorption (thus, the physisorption energy). On the other hand, the partially negatively charged surface of the Mo_2C, facilitates the activation of CO_2, and the adsorption of electrophilic species, such as atomic oxygen.[62]

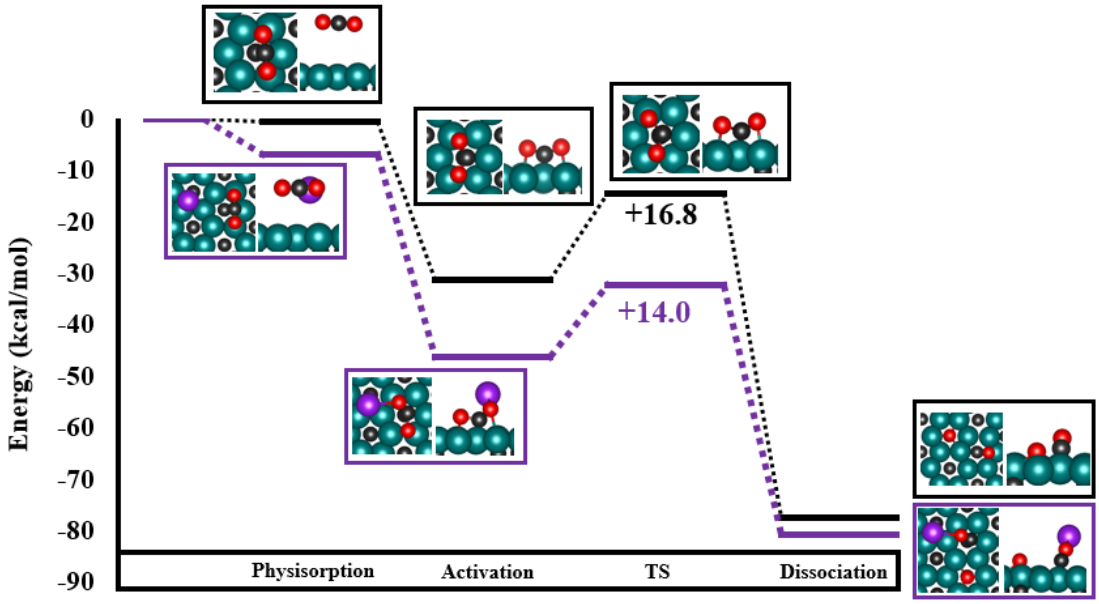

Figure 6. CO_2 dissociation profiles on Mo-terminated, pristine (black) and K-promoted (purple), β-Mo_2C(001) surfaces (energy in kcal mol-1). Color code: grey-C, cyan-Mo, red-O, purple-K.

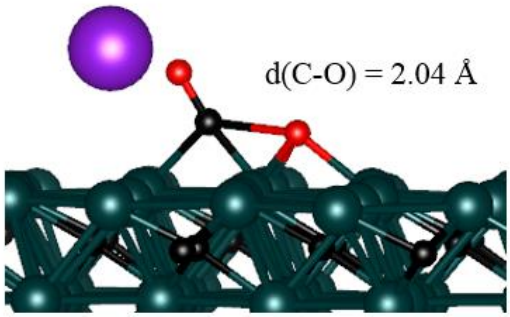

Figure 7: Transition state (T.S.) for CO_2 dissociation on K doped Mo-terminated (001) surface. Color code: grey-C, cyan-Mo, red-O, purple-K

Since the dissociation of CO_2 on K-doped Mo-terminated Mo_2C (001) is thermodynamically favorable, we conducted a CI-NEB calculation to study the actual dissociation pathway and locate T.S. In Figure 6, CO_2 dissociation profiles on both pristine and K-promoted Mo_2C (001) surfaces are presented and compared. On the K-promoted, Mo-

terminated surface (purple), CO_2 is first barrierlessly activated to a chemisorbed state (-46.6 kcal/mol), and then dissociates to CO and O with a barrier of 14.0 kcal/mol. The bond length of C-O of the T.S. was 2.04 Å (Figure 7). All of these steps are again exothermic with respect to the initial, CO_2 physisorbed state. It is worth noting that the barrier for CO_2 to dissociate from the activated state to CO* + O* in the presence of K is 2.8 kcal mol^{-1} lower than that of the pristine β-Mo_2C(001) surface. Taking into consideration the decrease in activation energy for CO_2 dissociation and the increase of the CO_2 physisorption on the Mo-terminated, β-Mo_2C(001) surface in the presence of K, it is apparent that K doping facilitates the formation of CO. These DFT calculated reaction barriers are in excellent agreement with those obtained experimentally, as shown in Table 3.

Table 3. Comparison of theoretical activation barrier (Ea) calculated by DFT and experimentally determined apparent activation barrier (Ea_app) for CO formation from CO_2 over pristine and K-promoted Mo_2C-based catalysts. (kcal/mol)

	Theoretical Ea	**Experimental Ea_{app}**
Pristine (No K) Mo_2C	16.8	14.0
K-Promoted Mo_2C	14.0	11.4

3.3 CO_2 ADSORPTION BEHAVIOR ON O-COVERED MO_2C (001) SURFACE

Under experimental conditions, and based on the affinity of Mo_2C to dissociate CO_2, the metal carbide surface may be converted to an oxygenated carbide surface. Also, the surface oxygen is likely to be produced by dissociative adsorption of H_2O molecule under RWGS conditions.[63] As a result, we calculated the binding energy of oxygen on five different oxygen surface coverages ranging from 0.25 ML (monolayer) to 1.25 ML, as shown in Figure 8. The binding energy of oxygen was calculated by equation (3-1):

$$E(O)=E(nO\text{-surf}) - nE(H_2) - nE(H_2O) \quad (3\text{-}1)$$

where n is the number of oxygen atoms adsorbed in one super cell. The optimized O-covered Mo_2C (001) surface are shown in Figure 8. The most preferred adsorption site for oxygen atom was found to be the hollow site, where the oxygen atom is stabilized by three surface Mo atoms. At one ML O-coverage, all of the hollow sites have been occupied by oxygen, and therefore further addition of more oxygen atoms to the surface are expected to be of higher energy. From Figure 9, one can observe that the binding energy of oxygen increases (more exothermic) as the O-coverage increases, and this trend was found to be changed when the surface O-coverage is greater than 1 ML (decrease in binding energy).

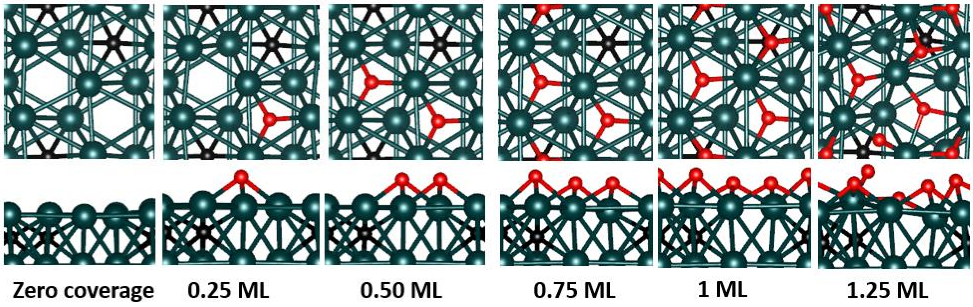

Figure 8. (from left to right) Optimized O-Mo_2C (001) surfaces at 0.00ML (clean surface), 0.25ML, 0.50ML, 0.75ML, 1ML, and 1.25ML oxygen coverage. (up: top view; bottom: side view)

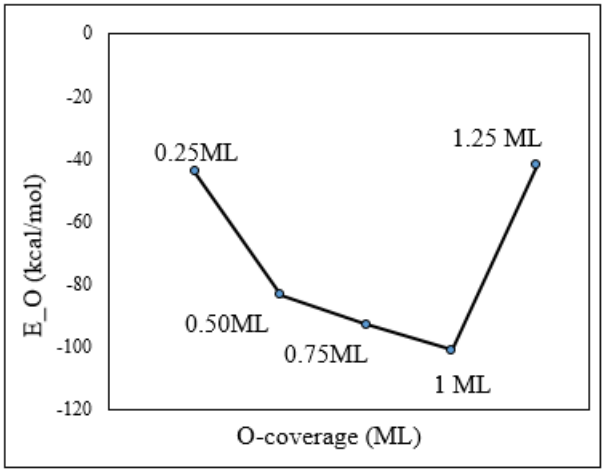

Figure 9. Binding energy of oxygen at a given coverage from 0.25 ML to 1.25 ML (Mo-terminated Mo_2C).

It is interesting to see that how the CO_2 adsorption behavior changes with surface O-coverage. As noted earlier, on clean β-Mo_2C (001) surface, the most preferential site for CO_2 chemisorption is found to be the hollow site. However, on O-covered surfaces, some of these sites may be occupied by oxygen, and therefore, different sites must be investigated in order to obtain the most stable chemisorption configuration of CO_2. On 0.25 ML O-coverage, three different sites (shown in Figure 10) were observed to be capable of activating CO_2, with the strongest binding energy at the hollow site (-18.8 kcal/mol). The O-C-O bond angle of activated

CO_2 was 134.2 degrees, and the C-O bond length was 1.27 Å. The average Mo-O distance is 2.37 Å.

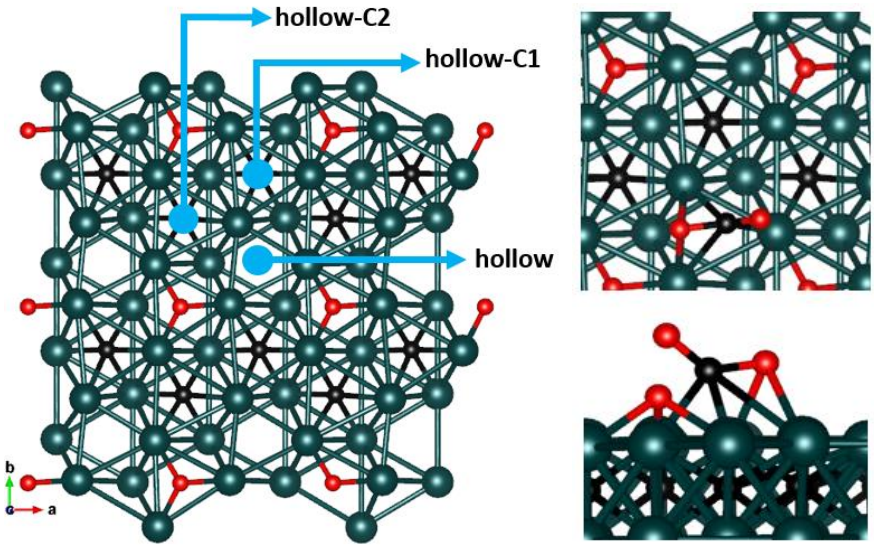

Figure 10. (left) Top view of 0.25ML O-Mo_2C(001), with 3 adsorption sites pointed in blue. (right) CO_2 adsorption on 0.25ML O-Mo_2C (001) surface at hollow site (up: top view, bottom: side view). The O-C-O bond angle of activated CO_2 was 134.2 degrees, and the bond length was 1.27 Å

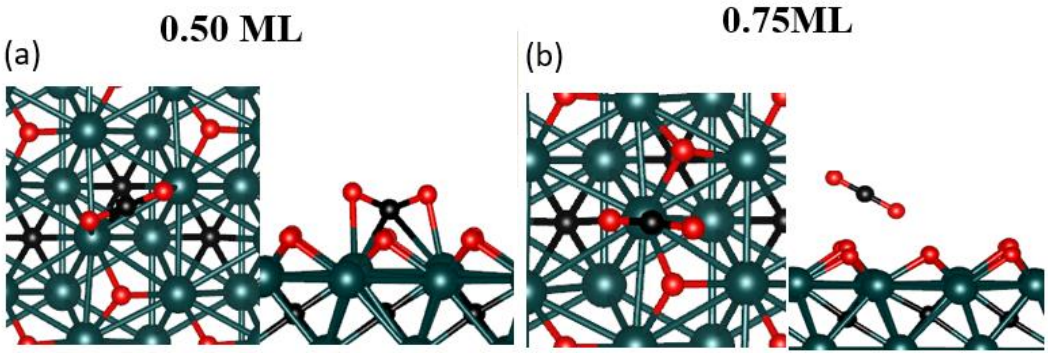

Figure 11: CO_2 adsorption on (a) 0.50ML and (b) 0.75ML O-Mo_2C(001) (left: top view, right: side view).

On 0.5 ML O-covered surface, the hollow site was found to activate CO_2 with BE of -5.37 kcal/mol, which shows weaker binding compared to that on 0.25 ML (-18.8 kcal/mol) and

clean surface (-29.8 kcal/mol). The O-C-O bond angle of activated CO_2 was 137.5 degrees, and the C-O bond length was 1.25 Å. The average Mo-O length was 2.31 Å.

On 0.75 ML O-covered surface, no chemisorption of CO_2 was obtained, and a positive BE of +12.0 kcal/mol was noted, indicating that the interaction of CO_2 becomes endothermic at high O-coverage surfaces. The activation/adsorption of CO_2 on 0.5 ML and 0.75 ML O-covered surfaces are shown in Figure 11.

Figure 12 summaries the binding energy of CO_2 vs. O-coverage. One can observe that the binding energy of CO_2 follows a linear trend: the lower the O-coverage, the stronger the CO_2 adsorption (larger negative BE (CO_2) values). However, at O-coverage larger than 0.75 ML, the interaction of CO_2 with the surface becomes endothermic, the adsorption of CO_2 is no longer favorable.

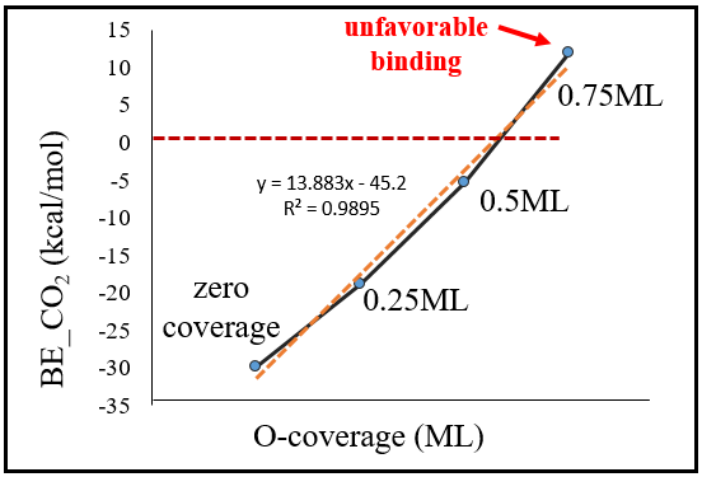

Figure 12. Binding energy of CO_2 (BE_CO_2) vs. O-coverage on Mo_2C (001) surface (the most preferred binding sites on each O-coverage surface).

To find the activation energy for CO_2 dissociation, CI-NEB calculations were carried out. Several CO_2 dissociated (CO*+O*) configurations were constructed as described below: holding the CO* at a particular site, and varying the location of O* at neighboring sites, and minimize the total energies of these different configurations. After obtaining the most stable dissociated configuration, this structure was considered as the final state (dissociated CO_2) for CI-NEB calculations, and the corresponding reaction path was then constructed. Figure 13 and 14 showed the CO_2 dissociation profiles on 0.25ML and 0.5ML O-Mo_2C surfaces (surfaces that still chemisorb CO_2). The activation barriers on 0.25ML and 0.50ML O-Mo_2C surfaces are 23.57 kcal/mol and 26.89 kcal/mol, respectively. The distances of O-CO bond of the T.S. are 1.750 Å (0.25ML) and 1.753 Å (0.50ML).

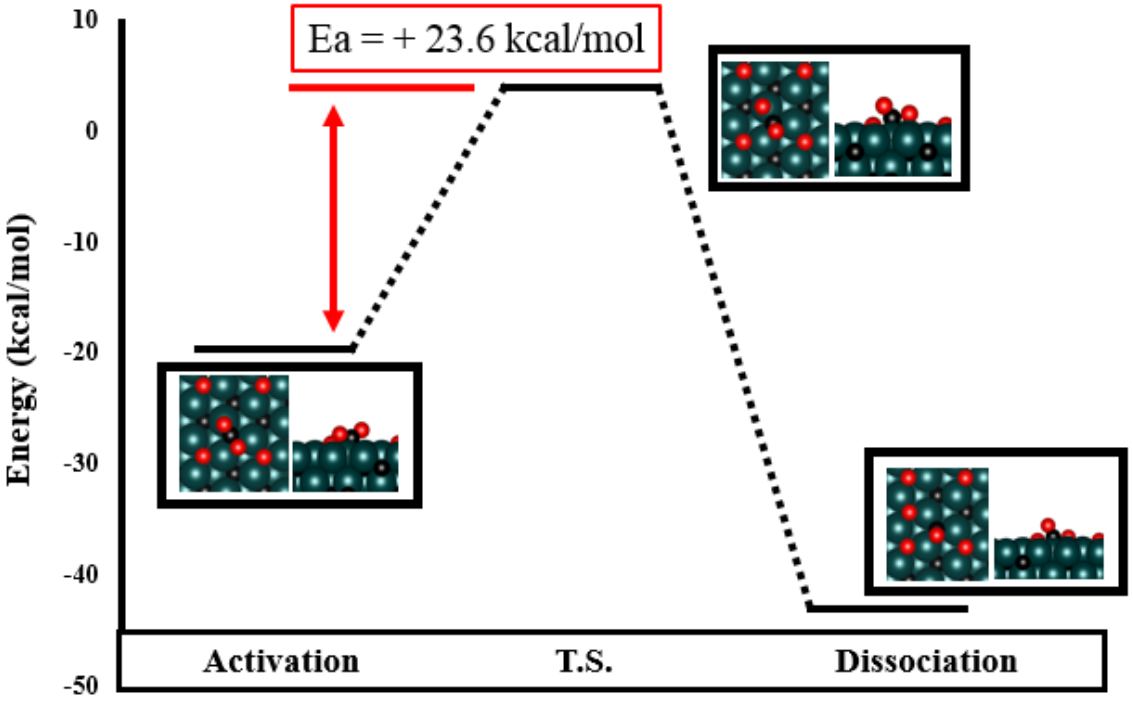

Figure 13: CO_2 dissociation profile at hollow site on 0.25 ML O-Mo_2C surface

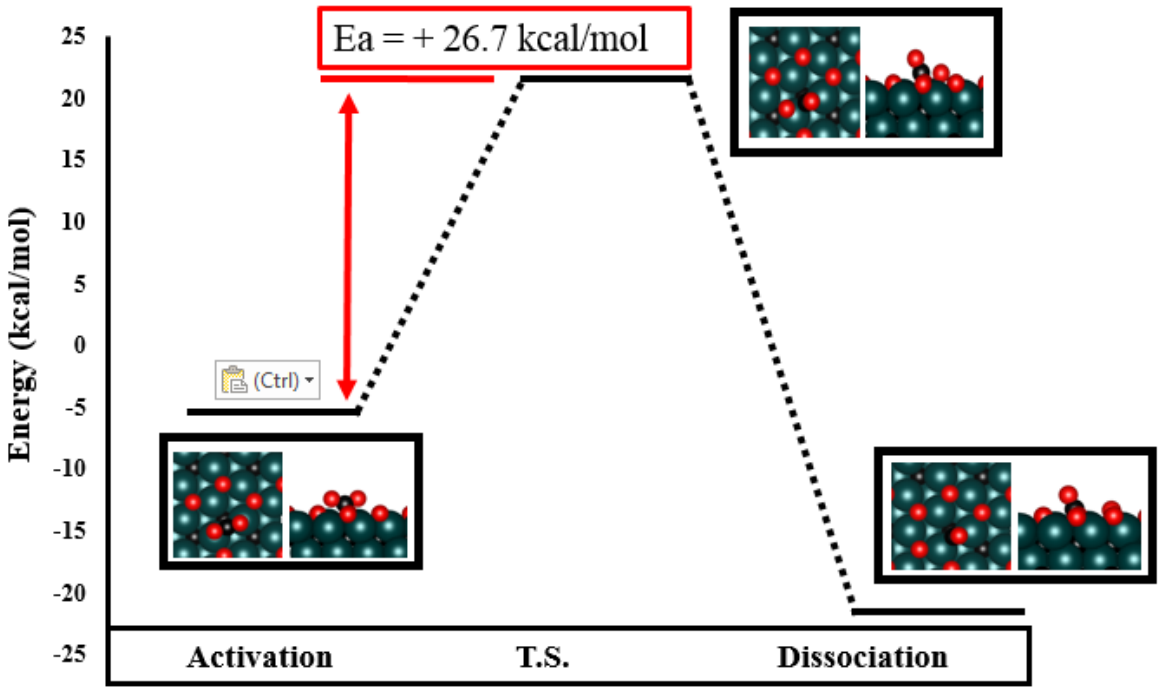

Figure 14: CO_2 dissociation profile at hollow site on 0.5 ML O-Mo_2C surface

In Figure 15 we summarize the activation energy of CO_2 dissociation (kcal/mol) on (1) pristine surface, (2) K-doped surface, (3) 0.25 ML O-covered, and (4) 0.50 ML O-covered Mo_2C (001) surface. We found by our NEB calculations that, while the presence of surface K atom decrease the activation energy of CO_2 dissociation, surface O atoms have a different effect on CO_2 adsorption behavior on Mo_2C(001) surface. The activation energy of CO_2 dissociation increases as O-coverage increases, which is in line with the binding energy calculations of CO_2 and oxygen on surfaces with different O-coverage (the weaker the CO_2 binding, the higher the CO_2 dissociation barrier). Surface K atom acts as an electron doner, loses almost one electron, and thus creates the partially negatively charged Mo_2C surface and enhances adsorption of CO_2. O atoms, however, stay at active sites for CO_2 adsorption, and form Mo oxide, which can

introduce repulsion to the adsorbents containing oxygen, and consequently decrease the adsorption of CO_2 on the surface.

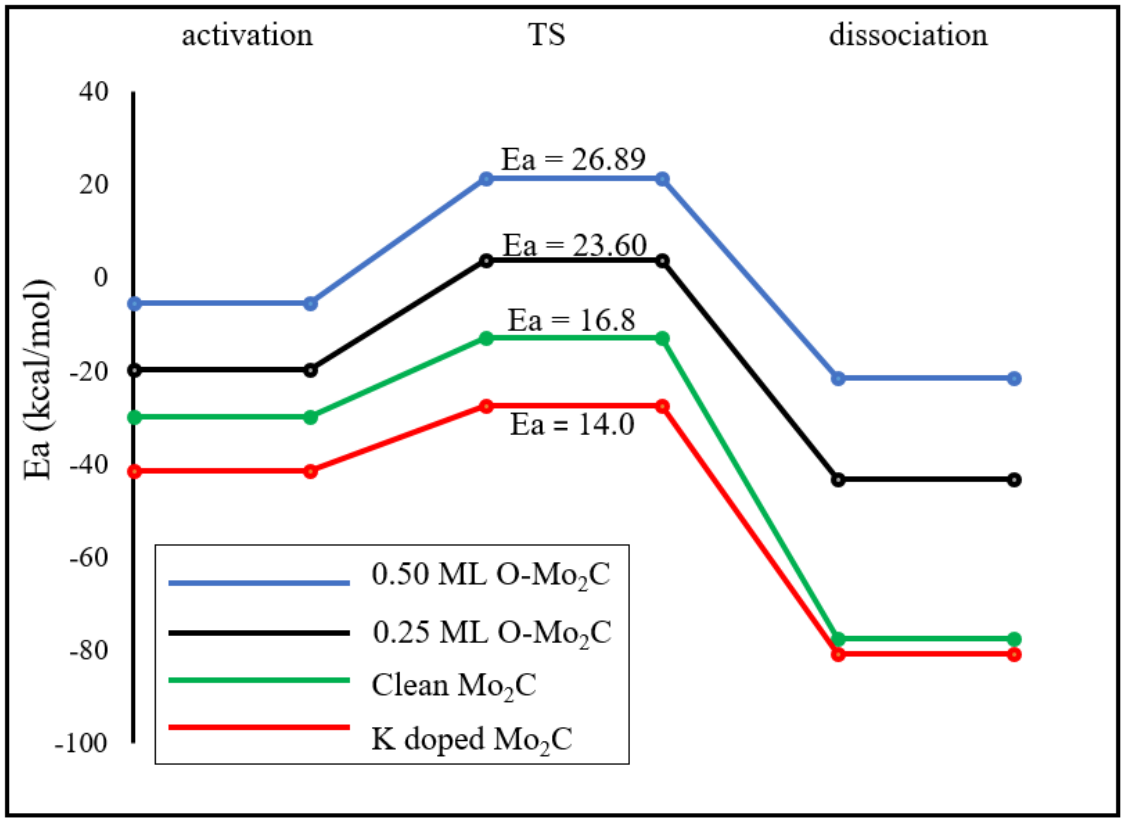

Figure 15. CO_2 dissociation profiles on pristine surface (green), K-doped surface (red), 0.25 ML O-covered (black), and 0.50 ML O-covered surface (blue). Ea represents activation energy in kcal/mol.

4.0 CONCLUSIONS

The adsorption behavior of CO_2 on β-Mo_2C (001) was studied, and the effects of K promotion and oxygen coverage on adsorption and dissociation of CO_2 have been investigated. On clean β-Mo_2C (001) surface, CO_2 undergoes a barrierless activation, with a binding energy of -31.4 kcal/mol, and dissociated to CO* and O* with an activation barrier of 16.8 kcal/mol. When the surface is promoted by K atom, the changes in the charges surface atoms results in a stronger binding of CO_2 (-46.4 kcal/mol) and CO_2 dissociates through a lower activation barrier (14.0 kcal/mol). Under experimental conditions, the surface is likely to be covered with oxygen atoms, and therefore the effect(s) of O-coverage on Mo_2C (001) were also studied. According to our results, the binding of oxygen on the surface increases as the surface coverage increases, until it reaches a maximum at 1ML coverage. Then, further oxygen adsorption becomes unfavorable (decrease in oxygen adsorption energy). CO_2 binding energy decreases with the increase in surface oxygen atoms, therefore, CO_2 can no longer strongly chemisorb at high oxygen coverage (O-coverage > 0.5ML). We show that the activation barriers for CO_2 dissociation also increase as O-coverage increases. Finally, it should be noted that even though the Mo_2C surface can become an oxy-Mo_2C surface, under reaction conditions, our study shows that CO_2 can still adsorb and dissociate at low O-coverage (<0.50ML).

APPENDIX A

EXAMPLE OF VASP INPUT FILES

1. INCAR (CI-NEB) (8 intermediate images for example)

```
SYSTEM = NEB_for_test2_1
ENCUT  = 415
PREC   = ACC
ISTART = 0
ICHARG = 2
#ISPIN  = 2 !spin polarized calculation, collinear
#MAGMOM = 32*0.6 48*0.6 3*2 8*2
NELM   = 100
NELMIN = 8
NELMDL = -15
EDIFF  = 1.0E-6
ISMEAR = 1
SIGMA  = 0.2
EDIFFG = -0.01
ISIF   = 2

IBRION = 3
POTIM  = 0
# IVDW = 12
NPAR = 8

NSW    = 1000
LREAL  = A
 ALGO  = Fast
ADDGRID = .TRUE.
ALGO = Fast
# IALGO  = 48
#IALGO  = 38
# NSIM   = 4
# NPAR   = 2
# NCORE  = 12
# NCORE  = 4
LPLANE = .TRUE.
LSCALU = .FALSE.
ISYM  = 0
#SYMPREC = 1.0E-5
LWAVE  = .FALSE.
LCHARG = .FALSE.
ICHAIN = 0
IMAGES = 8
LCLIMB = .TRUE.
```

INVCURV= 0.01
MAXMOVE= 0.1
SPRING = -5
IOPT = 1

MIXING
AMIX = 0.2
BMIX = 0.0001
AMIX_MAG = 0.8
BMIX_MAG = 0.0001

2. INCAR (GEOMETRY OPTIMIZATION)

```
SYSTEM = Co2C_unit_cell

 ISTART = 0
 ICHARG = 2
 ENCUT  = 415
 EDIFF = 10E-5
 EDIFFG = -0.01
 NSW = 600
 IBRION = 2
 POTIM = 0.5
 ISMEAR = 1
 SIGMA = 0.2
 LORBIT=11
 ISIF = 2
 ISPIN= 2

# MAGMOM = 12*2.73 6*0.6
# KSPACING = 0.3
# KGAMMA = .TRUE.

 NPAR = 8
```

3. KPOINTS FILE

```
k-points
 0
Monkhorst Pack
5 5 1
0 0 0
```

4. POSCAR FILE (COORDINATES)

Example: system: CO2 adsorption on 0.25ML O-covered surface. The supercell contains 32 Mo, 17 C, and 6 O atoms. Bottom two atom layers are frozen.

```
025_CO2
   1.00000000000000
    10.5006999968999999    0.0000000000000000    0.0000000000000000
     0.0000000000000000   12.1464004516999999    0.0000000000000000
     0.0000000000000000    0.0000000000000000   14.5508003235000007
   Mo   C    O
    32   17     6
Selective dynamics
Direct
  0.4089901121250875  0.4138433939748368  0.2327324038002399   T   T   T
  0.3354400099999992  0.2802599970000017  0.0798399970000006   F   F   F
  0.1706767613960778  0.2840791025895198  0.2371932394341624   T   T   T
  0.0854400019999986  0.4092200099999985  0.0833299980000035   F   F   F
  0.1571365542600798  0.0294400432882011  0.2334426789999201   T   T   T
  0.0854400019999986  0.1592199950000008  0.0798399970000006   F   F   F
  0.4298335768171378  0.1462546714021445  0.2299415137326262   T   T   T
  0.3354400099999992  0.0302599999999984  0.0833299980000035   F   F   F
  0.9082699154462386  0.4150655722940223  0.2291086048616944   T   T   T
  0.8354399799999968  0.2802599970000017  0.0798399970000006   F   F   F
  0.6700133995115881  0.2794636427364713  0.2357875586014058   T   T   T
  0.5854399799999968  0.4092200099999985  0.0833299980000035   F   F   F
  0.6563675218506807  0.0264539538526661  0.2322777378701789   T   T   T
  0.5854399799999968  0.1592199950000008  0.0798399970000006   F   F   F
  0.9305292865999015  0.1450844837937448  0.2305478844298068   T   T   T
  0.8354399799999968  0.0302599999999984  0.0833299980000035   F   F   F
  0.4027903280383004  0.9149510794893511  0.2287900826437061   T   T   T
  0.3354400099999992  0.7802600260000006  0.0798399970000006   F   F   F
  0.1645767641944413  0.7831936454790900  0.2376986549950102   T   T   T
  0.0854400019999986  0.9092199800000031  0.0833299980000035   F   F   F
  0.1515353847049718  0.5264023538777882  0.2322109688287451   T   T   T
  0.0854400019999986  0.6592199800000031  0.0798399970000006   F   F   F
  0.4146821629585720  0.6584340449790593  0.2386635686672430   T   T   T
  0.3354400099999992  0.5302600260000006  0.0833299980000035   F   F   F
  0.9046164365401494  0.9161727120557551  0.2306478949435299   T   T   T
  0.8354399799999968  0.7802600260000006  0.0798399970000006   F   F   F
  0.6690672160953979  0.7825308576340650  0.2375123164149738   T   T   T
```

0.5854399799999968	0.9092199800000031	0.0833299980000035	F	F	F
0.6544243651298871	0.5262881216821537	0.2369868687148877	T	T	T
0.5854399799999968	0.6592199800000031	0.0798399970000006	F	F	F
0.9268162692892351	0.6476094681641777	0.2310208189664110	T	T	T
0.8354399799999968	0.5302600260000006	0.0833299980000035	F	F	F
0.2500000000000000	0.4081600009999988	0.0000000000000000	F	F	F
0.0010537975995928	0.2836611066035502	0.1644614150195041	T	T	T
0.0000000000000000	0.0313199980000007	0.0000000000000000	F	F	F
0.2512857546300574	0.1565691699302806	0.1635337516694853	T	T	T
0.7500000000000000	0.4081600009999988	0.0000000000000000	F	F	F
0.5007564371717087	0.2843431853042958	0.1642337538795328	T	T	T
0.5000000000000000	0.0313199980000007	0.0000000000000000	F	F	F
0.7516402588723645	0.1548345132880171	0.1634639209735805	T	T	T
0.2500000000000000	0.9081599710000035	0.0000000000000000	F	F	F
-0.0017873117864665	0.7840553400353719	0.1640471078622794	T	T	T
0.0000000000000000	0.5313199759999989	0.0000000000000000	F	F	F
0.2470603336520769	0.6561194884396151	0.1634433723066702	T	T	T
0.7500000000000000	0.9081599710000035	0.0000000000000000	F	F	F
0.5017403284308778	0.7826588632074278	0.1642497448280300	T	T	T
0.5000000000000000	0.5313199759999989	0.0000000000000000	F	F	F
0.7482340192474665	0.6549793198625016	0.1640458319473670	T	T	T
0.4692821217510015	0.5575438177146878	0.3456122380818236	T	T	T
0.2396837041156454	0.4093407981705208	0.3102216873172107	T	T	T
0.2412034148914359	0.9072125103773981	0.3098396767776814	T	T	T
0.7507613770308194	0.4025195057272736	0.3069790273612038	T	T	T
0.7427058991546281	0.9069804082963105	0.3105041706094213	T	T	T
0.24706	0.6561204266880118	0.3714307272806929	T	T	T
0.5328711562845345	0.4712176694574253	0.3669585335962396	T	T	T

BIBLIOGRAPHY

(1) Daniel A. Lashof, D. R. A. Relative contributions of greenhouse gas emissions to global warming. *Nature* **1990**, *344*, 529-531.

(2) Robert Mendelsohn, W. D. D., Daigee Shaw The impact of global warming on Agriculture: A Richardian analysis *The American Economic Review* **1994**, *84*, 753-771.

(3) Mikkelsen, M.; Jorgensen, M.; Krebs, F. C. The teraton challenge. A review of fixation and transformation of carbon dioxide. *Energy & Environmental Science* **2010**, *3*, 43-81.

(4) D'Alessandro, D. M.; Smit, B.; Long, J. R. Carbon dioxide capture: prospects for new materials. *Angewandte Chemie International Edition* **2010**, *49*, 6058-6082.

(5) T. M. L. Wigley, R. R., J.A. Edmonds Economic and environmental choices in the stabilization of atmosphere CO_2 concentrations. *Nature* **1996**, *379*, 240-243.

(6) Gillis, J. New York Times, 2013; Vol. 2013.

(7) Robert Socolow, M. D., Roger Aines, Jason Blackstock, Olav Bolland, Tina Kaarsberg, Nathan Lewis, Marco Mazzotti, Allen Pfeffer, Karma Sawyer, Jeffrey Siirola, Berend Smit, Jennifer Wilcox *Direct air capture of CO_2 with chemicals: a technology assessment for the APS Panel on public affairs*, American Physical Society 2011.

(8) Song, C. Global challenges and strategies for control, conversion and utilization of CO_2 for sustainable development involving energy, catalysis, adsorption and chemical processing. *Catalysis Today* **2006**, *115*, 2-32.

(9) Wang, W.; Wang, S.; Ma, X.; Gong, J. Recent advances in catalytic hydrogenation of carbon dioxide. *Chemical Society Reviews* **2011**, *40*, 3703-3727.

(10) Mikkelsen, M.; Jørgensen, M.; Krebs, F. C. The teraton challenge. A review of fixation and transformation of carbon dioxide. *Energy & Environmental Science* **2010**, *3*, 43-81.

(11) Porosoff, M. D.; Yang, X.; Boscoboinik, J. A.; Chen, J. G. Molybdenum carbide as alternative catalysts to precious metals for highly selective reduction of CO_2 to CO. *Angewandte Chemie International Edition* **2014**, *53*, 6705-6709.

(12) Rochelle, C. A.; Czernichowski-Lauriol, I.; Milodowski, A. E. The impact of chemical reactions on CO_2 storage in geological formations: a brief review. *Geological Society, London, Special Publications* **2004**, *233*, 87-106.

(13) Yu, C.-H. A Review of CO_2 Capture by Absorption and Adsorption. *Aerosol and Air Quality Research* **2012**, *12*, 745-769.

(14) Steeneveldt, R.; Berger, B.; Torp, T. A. CO_2 Capture and Storage: closing the Knowing-Doing gap. *Chemical Engineering Research and Design* **2006**, *84*, 739-763.

(15) Haszeldine, R. S. Carbon Capture and Storage: How Green Can Black Be? . *Science* **2009**, *325*, 1647-1652.

(16) Resnik, K. P. Aqua Ammonia Process for Simultaneous Removal of CO_2, SO_2 and NOx. *Int. J. Environ. Technol. Manage.* **2004**, *4*, 89-104.

(17) Davis, J.; Rochelle, G. Thermal degradation of monoethanolamine at stripper conditions. *Energy Procedia* **2009**, *1*, 327-333.

(18) Welton, T. Room-temperature ionic liquids. Solvents for synthesis and catalysis. *Chem. Rev.* **1999**, *99*, 2071-2083.

(19) Eleanor D. Bates, R. D. M., Ioanna Ntai, and James H. Davis, Jr. CO_2 Capture by a Task-Specific Ionic Liquid. *J. AM. CHEM. SOC.* **2002**, *124*, 926-927.

(20) Zhang, Y.; Zhang, S.; Lu, X.; Zhou, Q.; Fan, W.; Zhang, X. Dual amino-functionalised phosphonium ionic liquids for CO_2 capture. *Chemistry* **2009**, *15*, 3003-3011.

(21) Jianbin Tang, W. S., Huadong Tang, Maciej Radosz, Youqing Shen Enhanced CO_2 absorption of Poly(ionic liquid)s. *Macromolecules* **2005**, *38*, 2037-2039.

(22) Ferdi Karadas, M. A., Santiago Aparicio Review on the Use of Ionic Liquids (ILs) as Alternative Fluids for CO_2 Capture and Natural Gas Sweetening. *Energy Fuels* **2010**, *24*, 5817-5828.

(23) Ramshaw, C. R., GB2), Mallinson, Roger H. (Runcorn, GB2); Imperial Chemical Industries Limited (London, GB2): United States, 1981.

(24) Hwai-Shen Liu, C.-C. L., Sheng-Chi Wu, and Hsien-Wen Hsu Characteristics of a Rotating Packed Bed. *Ind. Eng. Chem. Res.* **1996**, *35*, 3590-3596.

(25) Jian-Feng Chen, Y.-H. W., Fen Guo, Xin-Ming Wang, and Chong Zheng Synthesis of Nanoparticles with Novel Technology: High-Gravity Reactive Precipitation. *Ind. Eng. Chem. Res.* **2000**, *39*, 948-954.

(26) Sarat Munjal, M. D., Palghat Ramachandran Mass-transfer in rotating packed beds: development of gas-liquid and liquid-solid mass-transfer correlations. *Chemical engineering Science* **1989**, *44*, 2245-2256.

(27) Majeed S. Jassim, G. R., Dag Eimer, and Colin Ramshaw| Carbon Dioxide Absorption and Desorption in Aqueous Monoethanolamine Solutions in a Rotating Packed Bed. *Ind. Eng. Chem. Res.* **2007**, *46*, 2823-2833.

(28) Wei, W.; Jinlong, G. Methanation of carbon dioxide: an overview. *Frontiers of Chemical Science and Engineering* **2010**, *5*, 2-10.

(29) Gargiulo, N.; Pepe, F.; Caputo, D. CO_2 Adsorption by Functionalized Nanoporous Materials: A Review. *Journal of Nanoscience and Nanotechnology* **2014**, *14*, 1811-1822.

(30) Choi, S.; Drese, J. H.; Jones, C. W. Adsorbent materials for carbon dioxide capture from large anthropogenic point sources. *ChemSusChem* **2009**, *2*, 796-854.

(31) Hongqun Yang, Z. X., Maohong Fan, Rajender Gupta, Rachid B Slimane, Alan E Bland4, Ian Wright Progress in carbon dioxide separation and capture: A review. *Journal of Environmental Sciences* **2008**, *20*, 14-27.

(32) Simone Cavenati, C. A. G., and Alı´rio E. Rodrigues Adsorption Equilibrium of Methane, Carbon Dioxide, and Nitrogen on Zeolite 13X at High Pressures. *J. Chem. Eng. Data* **2004**, *49*, 1095-1101.

(33) Hailian Li, M. E., M. O'Keeffe, O. M. Taghi Design and synthesis of an exceptionally stable and highly porous metal-organic framework. *Nature* **1999**, *402*, 276-279.

(34) Mohamed Eddaoudi, J. K., Nathaniel Rosi, David Vodak, Joseph Wachter, Michael O'Keeffe, Omar M. Yaghi Systematic Design of Pore Size and Functionality in Isoreticular MOFs and Their Application in Methane Storage. *Science* **2002**, *295*, 469-472.

(35) Yaghi, A. R. M. a. O. M. Metal-Organic Frameworks with Exceptionally High Capacity for Storage of Carbon Dioxide at Room Temperature. *J. AM. CHEM. SOC.* **2005**, *127*, 17998-17999.

(36) Qing Xu, D. L., Qingyuan Yang, Chongli Zhong, Jianguo Mi Li-modified metal-organic frameworks for CO_2/CH_4 separation: a route to achieving high adsorption selectivity. *Journal of Materials Chemistry* **2009**, *20*, 706-714.

(37) Youn-Sang Bae, O. K. F., Alexander M. Spokoyny, Chad A. Mirkin, Joseph T. Hupp, Randall Q. Snurr Carborane-based metal-organic frameworks as highly selective sorbents for CO_2 over methane. *Chem. Commun* **2008**, 4135-4137.

(38) Hee K. Chae , D. Y. S.-P. r., Jaheon Kim, YongBok Go, Mohamed Eddaoudi, Adam J. Matzger, Michael O'Keeffe & Omar M. Yaghi A route to high surface area, porosity and inclusion of large molecules in crystals. *Nature* **2004**, *427*, 523-527.

(39) Banerjee, R.; Phan, A.; Wang, B.; Knobler, C.; Furukawa, H.; O'Keeffe, M.; Yaghi, O. M. High-throughput synthesis of zeolitic imidazolate frameworks and application to CO_2 capture. *Science* **2008**, *319*, 939-943.

(40) Saeidi, S.; Amin, N. A. S.; Rahimpour, M. R. Hydrogenation of CO_2 to value-added products—A review and potential future developments. *Journal of CO_2 Utilization* **2014**, *5*, 66-81.

(41) Shou, H.; Davis, R. J. Reactivity and in situ X-ray absorption spectroscopy of Rb-promoted Mo_2C/MgO catalysts for higher alcohol synthesis. *Journal of Catalysis* **2011**, *282*, 83-93.

(42) J. R. Rostrup-Niesen, J. B. H. CO_2-reforming of methane over transition metals. *Journal of Catalysis* **1992**, *144*, 38-49.

(43) Dry, M. E. The Fischer–Tropsch process: 1950–2000. *Catalysis Today* **2002**, *71*, 227-241.

(44) Robert W. Dorner, D. R. H., Frederick W. Williams, Burtron H. Davis, and Heather D. Willauer Influence of Gas Feed Composition and Pressure on the Catalytic Conversion of CO_2 to Hydrocarbons Using a Traditional Cobalt-Based Fischer-Tropsch Catalyst. *Energy $ Fuels* **2009**, *23*, 4190-4195.

(45) Iglesia, E. Design, synthesis, and use of cobalt-based Fischer-Tropsch synthesis catalysts *Applied Catalysis A: General* **1997**, *161*, 59-78.

(46) Andrei Y. Khodakov, W. C., and Pascal Fongarland Advances in the Development of Novel Cobalt Fischer−Tropsch Catalysts for Synthesis of Long-Chain Hydrocarbons and Clean Fuels. *Chem. Rev.*, **2007**, *107*, 1692-1744.

(47) Zhao, S.; Liu, X.-W.; Huo, C.-F.; Li, Y.-W.; Wang, J.; Jiao, H. Surface morphology of Hägg iron carbide (χ-Fe_5C_2) from ab initio atomistic thermodynamics. *Journal of Catalysis* **2012**, *294*, 47-53.

(48) John B. Claridge, A. P. E. Y., Attila J. Brungs, Carlos Marquez-Alvarez, Jeremy Sloan, Shik Chi Tsang, and Malcolm L. H. Green New Catalysts for the Conversion of Methane to Synthesis Gas: Molybdenum and Tungsten Carbide. *Journal of Catalysis* **1998**, *180*, 85-100.

(49) Posada-Perez, S.; Vines, F.; Ramirez, P. J.; Vidal, A. B.; Rodriguez, J. A.; Illas, F. The bending machine: CO_2 activation and hydrogenation on delta-MoC(001) and beta-Mo_2C(001) surfaces. *Phys Chem Chem Phys* **2014**, *16*, 14912-14921.

(50) James C. Schlatter, S. T. O., Joseph E. MetcalfeIII, Joseph M. LambertJr. Catalytic behavior of selected transition metal carbides, nitrides, and borides in the hydrodenitrogenation of quinoline. *Ind. Eng. Chem. Res.* **1988**, *27*, 1648-1653.

(51) Furimsky, E. Metal carbides and nitrides as potential catalysts for hydroprocessing. *Applied Catalysis A: General* **2003**, *240*, 1-28.

(52) Oyama, S. R. a. S. T. New Catalysts for Hydroprocessing: Transition Metal Carbides and Nitrides *J. Phys. Chem.* **1995**, *99*, 16365-16372.

(53) Posada-Pérez, S.; Viñes, F.; Rodriguez, J. A.; Illas, F. Fundamentals of Methanol Synthesis on Metal Carbide Based Catalysts: Activation of CO2 and H2. *Topics in Catalysis* **2014**, *58*, 159-173.

(54) Rodriguez, J. A.; Liu, P.; Stacchiola, D. J.; Senanayake, S. D.; White, M. G.; Chen, J. G. Hydrogenation of CO_2 to Methanol: Importance of Metal–Oxide and Metal–Carbide Interfaces in the Activation of CO_2. *ACS Catalysis* **2015**, *5*, 6696-6706.

(55) Pistonesi, C.; Pronsato, M. E.; Bugyi, L.; Juan, A. The adsorption of CO on potassium doped molybdenum carbide surface: An ab-initio study. *Catalysis Today* **2012**, *181*, 102-107.

(56) Kresse, F. Efficient iterative schemes for ab initio total-energy calculations using a plane-wave basis set. *Physical Review B* **1996**, *54*, 11169-11186.

(57) Perdew, B., Ernzerho Generalized Gradient Approximation Made Simple. *Physical Review* **1996**, *77*, 3865-3868.

(58) Kitchin, J. R.; Nørskov, J. K.; Barteau, M. A.; Chen, J. G. Trends in the chemical properties of early transition metal carbide surfaces: A density functional study. *Catalysis Today* **2005**, *105*, 66-73.

(59) Pack, J. D.; Monkhorst, H. J. "Special points for Brillouin-zone integrations"—a reply. *Physical Review B* **1977**, *16*, 1748-1749.

(60) Sheppard, D.; Terrell, R.; Henkelman, G. Optimization methods for finding minimum energy paths. *J Chem Phys* **2008**, *128*, 134106.

(61) Porosoff, M. D.; Baldwin, J. W.; Peng, X.; Mpourmpakis, G.; Willauer, H. D. Potassium-Promoted Molybdenum Carbide as a Highly Active and Selective Catalyst for CO_2 Conversion to CO. *ChemSusChem* **2017**.

(62) Austin, N.; Butina, B.; Mpourmpakis, G. CO_2 activation on bimetallic CuNi nanoparticles. *Progress in Natural Science: Materials International* **2016**, *26*, 487-492.

(63) Rodriguez, P. L. a. J. A. Water-Gas-Shift Reaction on Molybdenum Carbide Surfaces: Essential Role of the Oxycarbide. *J. Phys. Chem. B* **2006**, *110*, 19418-19425.